



VCU

Virginia Commonwealth University
VCU Scholars Compass

Theses and Dissertations


Graduate School

2021

Surface Characterization of Accident Tolerant Fuel Claddings Candidates After Prolonged Exposure to Steam Oxidation

Connor F. Donlan
Virginia Commonwealth University

Follow this and additional works at: <https://scholarscompass.vcu.edu/etd>

 Part of the [Nuclear Engineering Commons](#), and the [Other Materials Science and Engineering Commons](#)

© The Author

Downloaded from

<https://scholarscompass.vcu.edu/etd/6834>

This Thesis is brought to you for free and open access by the Graduate School at VCU Scholars Compass. It has been accepted for inclusion in Theses and Dissertations by an authorized administrator of VCU Scholars Compass. For more information, please contact libcompass@vcu.edu.

**Surface Characterization of Accident Tolerant Fuel Claddings Candidates After Prolonged
Exposure to Steam Oxidation**

A thesis submitted in partial fulfillment of the requirements for the degree of Master of Science
at Virginia Commonwealth University.

By

Connor Francis Donlan

Virginia Military Institute, Bachelor of Science

Director: Dr. Jessika Rojas,

Associate Professor, Department of Mechanical and Nuclear Engineering

Committee:

Dr. Jessika Rojas

Dr. Braden Goddard

Dr. Rajnikant Umretiya

Virginia Commonwealth University

Richmond, Virginia

December 2021

Acknowledgments

I would like to thank my advisor Dr. Jessika Rojas, whose support and mentorship have been invaluable to me. I would also like to thank Dr. Rajnikant Umretiya for his support and guidance throughout this whole process. I am thankful for all the help that they have given to me. I would like to thank the staff at the Nanomaterials Core Characterization Facility for their support and training. Additionally, I would like to thank Helge Heinrich at the University of Virginia for conducting TEM analysis and Jee Hyun Seong at the Massachusetts Institute of Technology for conducting steam oxidation.

To my family, I would not be where I am today without your love and support. Allison, your love and support are what have enabled me to accomplish this goal. To my parents, without your guidance, I would not be where I am today.

Table of Contents

Acknowledgments.....	i
Table of Contents.....	ii
List of Figures.....	iv
List of Tables.....	v
Chapter 1: Introduction, Motivation, and Research Objectives.....	1
1.1 Introduction.....	1
1.2 Motivation.....	4
1.3 Research Objectives.....	7
1.3.1 Objective 1: Determine the Wettability and Surface Roughness of selected ATF Cladding materials through contact profilometry and contact angle.....	7
1.3.2 Objective 2: Determine the Surface Chemistry and Microstructure of the selected ATF Cladding materials after steam oxidation.....	8
1.3.3 Objective 3: Preliminary determination of Mechanical Properties of the selected ATF Cladding materials.....	9
Chapter 2: Accident Tolerant Fuel Claddings Background and Significance.....	11
2.1 Nuclear Reactors.....	11
2.2 Zircaloy-2 and Zircaloy-4.....	11
2.3 Loss of Coolant Accidents.....	12
2.4 Accident Tolerant Fuel Claddings.....	13
2.5 FeCrAl Alloys.....	13

2.6 Chromium-Coated Zirconium alloys	15
2.7 Steam Oxidation.....	16
Chapter 3: Experimental Procedure	18
3.1 Materials and Preparation	18
3.2 Surface Characterization.....	20
3.3 Surface Chemistry and Microstructure	21
3.4 Mechanical Testing.....	27
Chapter 4: Results and Discussion.....	28
4.1 Surface Roughness and Wettability	28
4.2 Surface Chemistry.....	29
4.3 Mechanical Properties.....	38
Chapter 5: Conclusions and Future Works	40
References.....	41
Vita.....	50

List of Figures

Figure 1.1 FeCrAl ATF Cladding [16]	3
Figure 1.2 Coated Zircaloy ATF Cladding [16]	4
Figure 1.3 Oxide thickness as a function of aging temperatures and time [20].....	5
Figure 2.1 Oxidation Behavior of FeCrAl in Super-Heated Steam [9]	14
Figure 3.1 Oxidation Testing Facility [60]	18
Figure 3.2 Non-Oxidized Cladding.....	19
Figure 3.3 Oxidized Samples	19
Figure 3.4 Mitutoyo Surftest SJ-410 Testing Setup	21
Figure 3.5 Rame-Hart Contact Angle Testing Setup and Landed Drop.....	21
Figure 4.1 SEM Images of the cross sections and oxide layers of oxidized selected cladding materials	30
Figure 4.2 XRD Patterns for oxidized Zircaloy-4, Chromium-Coated Zircaloy-4, and C26M....	30
Figure 4.3 Element composition vs. Depth profile (sputter time) on the Oxidized Samples: (a) C26M (b) Zircaloy-4 (c) Chromium-Coated Zircaloy-4 with accompanying high resolution spectra at 20 minutes.....	31-32
Figure 4.4 TEM observation of C26M: (a) STEM image of the oxide layer formed on C26M with associated EDS chemical maps (b)EDS line scan across the oxide layer	33
Figure 4.5 TEM observation of Chromium-Coated Zircaloy-4: (a) STEM image of oxide layer formed on Chromium-Coated Zircaloy-4 with associated EDS chemical maps (b) STEM image with associated EDS line scan across the oxide layer.....	36
Figure 4.6 TEM observation of Zircaloy-4: (a) STEM image of oxide layer formed on Zircaloy-4 with associated EDS chemical maps (b) EDS line scan across oxide layer	37

List of Tables

Table 1.1 Chemical Composition of Zircaloy Claddings [8],[12]-[14]	2
Table 1.2 Weight gains and appearances of the oxidation sample surfaces during the 500°C steam testing [26]	6
Table 2.1 Mechanical Properties of C26M [56]	14
Table 2.2 Mechanical Properties of Chromium-Coated Zircaloy, Zircaloy-2, and Zircaloy-4 [58]	15
Table 2.3 Summary of Oxidation Environments and Results.....	17
Table 3.1 Polishing Procedure	20
Table 3.2 SiO ₂ Scanning Procedure.....	23
Table 3.3 C26M Scanning Procedure	24
Table 3.4 Chromium-Coated Zircaloy-4 Scanning Procedure	25
Table 3.5 Zircaloy-4 Scanning Procedure	26
Table 4.1 Roughness and Contact Angle Comparison Between As-Received and Oxidized Samples.....	29
Table 4.2 Hardness Comparison for As-Received and Oxidized samples	39

Abstract

Accident Tolerant Fuel Claddings are designed to improve fuel performance and safety in abnormal reactor conditions. The development of these cladding materials has become a top priority for the nuclear community, with incidents such as the Three Mile Island accident and the Fukushima Dai-chi accident. The development of these claddings has resulted in 2 subsections: coating current claddings or replacing cladding materials with new materials. The claddings studied in this thesis are a Zircaloy-4 cladding coated with chromium through physical vapor deposition, Zircaloy-4, and a FeCrAl alloy, C26M. This thesis assessed the surface chemistry, roughness, and wettability after extended exposure to a high-temperature steam environment. The surfaces of the materials were studied to determine the impact of the flowing steam on the material's oxidation. The results showed that both proposed cladding materials exhibited improved oxidation characteristics compared to the Zircaloy-4. The surface chemistry of the claddings evidenced the oxide layer with a thickness of 3 μm , 23 μm , and 150 nm for chromium-coated Zircaloy-4, substrate Zircaloy-4, and C26M, respectively. The results of the coated cladding were found to agree with previous research in where the chromia layer forms and protects the substrate from oxidation. The FeCrAl alloy, C26M, showed the oxide development of an external layer rich in iron, with a lower fraction of chromium and aluminum, and an internal layer rich in aluminum. The preliminary characterization of the materials' mechanical properties results also showed a decrease in hardness for all materials.

Keywords: Accident Tolerant Fuel (ATF), Physical Vapor Deposition (PVD), Zircaloy-4, Cr-coated

Chapter 1: Introduction, Motivation, and Research Objectives

1.1 Introduction

Nuclear energy is a strong solution to deal with rising global warming concerns. Nuclear reactors generate clean energy while reducing the emission of greenhouse gases of conventional power plants[1]–[4]. Additionally, with increasing demands on energy and rising costs in the oil markets, nuclear energy becomes an efficient choice in reducing a country’s dependence on fossil fuels [1]–[4]. While nuclear energy production offers many advantages over other sources, its growth has been hampered by public perception of safety and reliability. Poor public perception of safety stems from several major accidents. These accidents include the Three Mile Island accident, which negatively influenced American public opinion of nuclear reactors, and the Fukushima Dai-ichi accident, which affected international views, both of which were caused by a loss of coolant accident (LOCA) [5]–[9]. The latter event, in particular, led to the search for improved cladding materials that could provide a longer coping time in accident scenarios while providing improved performance in normal operating conditions.

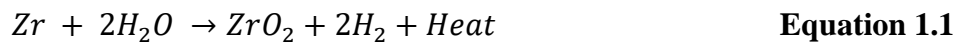
The Three Mile Island accident took place at the Three Mile Island Nuclear Station after a leakage in an electromagnetic relief valve resulted in a loss of coolant to the core. The issue was compounded by the fact that the operating staff did not recognize the issue for 2 hours [5], [6]. The accident led to substantial fuel damage and increased hydrogen production from the water and zirconium reaction [5], [6]. After the Three Mile Island accident, public perception of nuclear power and the creation of nuclear power decreased significantly in the United States [6]. Another substantial LOCA accident occurred at the Fukushima Dai-ichi nuclear power plant during the 2011 tsunami and earthquakes. These natural disasters left the reactor cores 1, 2, and 3 without coolant for an extended time. During this time, the heat generated from the reactors

caused an explosive reaction with the oxidation products from the fuel cladding material [7]–[9]. Zircaloy-2 and Zircaloy-4 are commercial nuclear fuel cladding materials in light water reactors (LWR) and have been used since the 1950s because of their low neutron absorption cross-section [8]. Pure zirconium has a negative oxidation reaction in a high-temperature steam environment; therefore, other metals are added to reduce the corrosion effects [8], [10], [11]. The chemical composition of these materials is shown in Table 1.1, with the primary difference between Zircaloy-2 and 4 being the Nickel and Iron content [8].

Table 1.1 Chemical Composition of Zircaloy Claddings [8], [12]–[14]

Material	Zircaloy-2	Zircaloy-4
	Weight Percent	
Sn	1.2-1.7	1.2-1.7
Fe	0.07-0.20	0.18-0.24
Cr	0.05-0.15	0.07-0.13
Ni	0.03-0.08	-
Average (Fe+Cr+Ni)	0.18-0.38	-
Average (Fe+Cr)	-	0.28-0.37
N, Max	0.008	0.008

The oxidation of the zirconium in the alloys under high-temperature steam environments, typically in the range of 550-1500 °C, can result in hydrogen gas and heat generation [8], [10], [11].



Hydrogen gas is highly reactive in atmospheres containing oxygen. The interaction of these two elements leads to a release of a large amount of energy that translates to a sharp explosion. These events were encountered in the Dai-Chi Nuclear Power plant accident [7]–[9]. The explosions also caused large amounts of radioactive material to be released into the environment. Since both

of these major incidents were caused by LOCAs there is a strong need for materials that can withstand abnormal reactor conditions.

According to the United States Office of Nuclear Energy, accident tolerant fuels are being designed for improved corrosion resistance, improved mechanical properties, and increased fuel efficiency [15]. Various alternative materials have been proposed and investigated in the nuclear industry to satisfy the requirements. According to the United States Nuclear Regulatory Commission (NRC), they have been categorized as near-term and longer-term technologies [16]. One of the near-term cladding materials being investigated is Iron-Chromium-Aluminum (FeCrAl) alloys. An example of a FeCrAl alloy is shown in Figure 1.1.



Figure 1.1 FeCrAl ATF Cladding [16]

FeCrAl alloys minimize hydrogen production under high-temperature steam conditions, significantly reducing potential explosions under accident scenarios. Furthermore, FeCrAl alloys have evidenced a slower oxidation rate than Zircaloy [17]. Additionally, this material has a desirable oxidation behavior that develops a specific oxide under certain environmental conditions, which helps to reduce further degradation of the substrate [18]. FeCrAl alloy cladding candidates can be reduced in thickness compared to a Zirconium cladding due to the physical properties of the alloy. This reduction in thickness allows for more uranium oxide fuel

to be inserted into a fuel rod to offset the higher neutron absorption cross-section of the material [17]. Another alternative cladding material that is also considered near-term is coated Zircaloy claddings. An example of a coated cladding is shown in Figure 1.2.



Figure 1.2 Coated Zircaloy ATF Cladding [16]

Coatings on the surface of the Zircaloy claddings aim to prevent the adverse oxidation of zirconium. In addition, this technology takes advantage of the already well-known characteristics and manufacturing process of the commercial Zircaloy cladding, which avoids substantial changes to either fuel pellets or fuel assemblies. Coating materials for ATF claddings tend to be chromium or metals that exhibit increased durability and oxidation resistance.

1.2 Motivation

This research investigates the changes in surface characteristics and oxide growth of selected cladding materials subjected to long-term exposure to high-temperature steam of 500 °C. This research is motivated by studies investigating the oxidation characteristics of coated Zircaloy and FeCrAl cladding materials. Terrani et al. determined oxidation behaviors of FeCrAl and Zircaloy materials for extended periods within water reactor environments to understand the oxidation kinetics [19]. The results showed that FeCrAl alloys with 10-15% Cr and 3-5% Al form a hematite scale on the surface [19]. Nan Li et al [20] oxidized C26M in stagnant air at

temperatures between 300 °C and 600 °C for times between 100 to 2000 hours. The study determined the microstructure and chemical composition of the samples and showed the formation of an oxide layer that follows a logarithmic time dependence and is shown in Figure 1.3 [20].

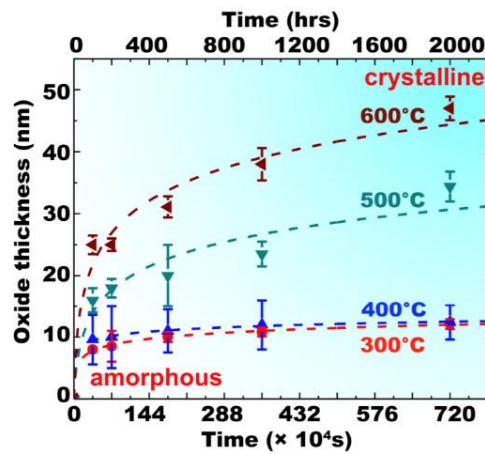






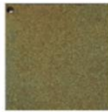
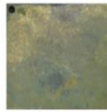

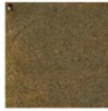
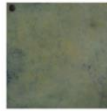

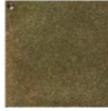

Figure 1.3 Oxide thickness as a function of aging temperatures and time [20]

Rebak et al. determined the oxidation behavior of FeCrAl alloys within super-heated steam environments at 1200 °C and pure water at 330 °C compared to traditional Zircaloy claddings [9].

Rebak et al. showed that as the temperature increases over 1100°C, the chromium layer volatilize. All results for stagnant air, steam, and water contact determined that the oxide pattern for FeCrAl alloys tends to follow the creation of a protective layer of chromium oxide first, then an aluminum oxide, and a hematite surface scaling which reduces the amount of iron being oxidized. [9], [17]–[23]. Umretiya et al. [24] explored the effects of chromium surface modifications on Zicaloy-4 through physical vapor deposition and cold spray. The coatings showed an increase in the mechanical strength of the samples and increased wettability of the surface [24]. Brachet et al. [25] oxidation of chromium-coated Zircaloy-4 in high-temperature,

high-pressure steam environments, ranging from 415 °C to 1100 °C, showed chromium-coated claddings had good corrosion resistance, fretting resistance, and resistance to high-temperature steam [25]. Seveck et al. [26] tested the oxidation behavior of Zircaloy-4, cold spray chromium-coated Zircaloy-4, and pure chromium in a 500 °C steam environment for an extended time between 1 to 20 days. The results showed that the coated samples cracked and allowed the substrate to oxidize, but the study was able to determine the weight gain of the samples in steam testing. The weight gain for the samples is shown in Table 1.2 [26].

Table 1.2 Weight gains and appearances of the oxidation sample surfaces during the 500 °C steam testing [26]

Exposition time		Zircaloy-4	Cr cold spray coating	Cr metal
1 day	Appearance			
4.3 days	Weight gain [mg/dm ²]	72.92	11.69	0.83
	Appearance			
11.6 days	Weight gain [mg/dm ²]	122.74	21.21	1.56
	Appearance			
20 days	Weight gain [mg/dm ²]	320.66	51.75	2.29
	Appearance			
	Weight gain [mg/dm ²]	586.56	94.18	2.43

Following previous reports on steam oxidation of ATF, this research determines the effects of high-temperature steam at 500 °C flowing over the material. The materials, as-received and oxidized, were characterized for their surface roughness, wettability, surface chemistry, and hardness. The surface chemistry of the claddings shows how the claddings oxidized within the environment and their impact on surface characteristics such as topography and affinity for water; the materials have desirable oxidation effects designed to limit their degradation and the

amount of H₂ created. The surface chemistry, microstructure, and chemical composition of the materials were characterized using photoelectric spectroscopy (XPS), X-ray diffractometry (XRD), scanning electron microscopy (SEM), transmission electron microscopy (TEM), and energy dispersive spectroscopy (EDS). Additionally, preliminary data were collected on hardness measurements to determine changes in mechanical properties due to the prolonged exposure to the steam environment.

1.3 Research Objectives

The overall objective of the research is to investigate the steam oxidation behavior of ATF claddings material candidates, including Cr-coated Zircaloy-4 and C26M FeCrAl alloy, compared to Zircaloy-4 upon exposure to a humid air flow of 2 standard cubic feet per hour at a temperature of 500 °C for 20 days in atmospheric pressure.

1.3.1 Objective 1: Determine the wettability and surface roughness of selected ATF cladding materials through contact profilometry and contact angle goniometry

The surface roughness and wettability of components used as heating elements have been evidenced to impact their heat transfer characteristics. As such, in the case of fuel claddings, these surface parameters may affect to some extent their thermohydraulic performance in reactor environments [27]. Additionally, the surface roughness may also affect the materials' oxidation behavior [28]. One of the current needs in developing accident tolerant fuel cladding materials is their improved reaction kinetics with steam, or minimizing oxidation rates, which occurs in design basis accidents where temperatures increase above 400 °C [9]. With the particular importance of oxidation behavior of ATF cladding candidates, there is a need to investigate and report their surface topography and wetting characteristics prior to steam oxidation. The surface wettability indicates the affinity between the surface and the fluid. A hydrophilic surface is a

surface with a static contact angle below 90° more inclined to interact with the liquid and improve rewetting in boiling. A hydrophobic surface is above 90° and tends to reject the fluid [29]–[31]. Furthermore, the surface roughness of the claddings may impact the wettability through surface tension and friction [29], [32]–[34]. All these surface parameters are then needed, along with oxidation behavior in specific environmental conditions. This stage is expected to serve as a foundation for future studies on the impact of surface characteristics on ATF oxidation.

The first objective is to investigate the surface characteristics of selected cladding candidates, as-received, using a set of materials characterization tools. The tasks followed to complete objective one are listed below.

Tasks:

1. Evaluate the surface roughness of the cladding candidate materials before and after steam oxidation using contact profilometry.
2. Evaluate the wettability of the cladding candidate materials before and after steam oxidation using contact angle goniometry.

1.3.2 Objective 2: Determine the surface chemistry and microstructure of the selected ATF cladding materials after steam oxidation

This objective investigates the oxidation behavior of the ATF claddings under steam conditions. The surface chemistry of the claddings after exposure to high-temperature steam shows how the claddings are reacting within the environment. The FeCrAl alloys have demonstrated their slower oxidation rates than Zr-based alloys and improved resistance to steam oxidation. This relies on their ability to form a Cr-rich oxide layer and alumina layer within

specific temperature intervals [35]. These oxide layers prevent further oxidation of the substrate materials with the environment [22], [36]. This oxidation pattern is useful because it significantly minimizes the rate of hydrogen generation. The coating on the Zircaloy claddings is designed to protect the underlying substrate and prevent rapid degradation in accident scenarios [37], [38]. For the coated claddings used in this work, chromium is deposited through Physical Vapor Deposition (PVD) on the surface of the Zircaloy-4.

This second specific objective aims to investigate the surface chemistry and microstructure of selected cladding candidates using a set of materials characterization tools. The tasks followed to complete objective 2 are listed below.

Tasks:

1. Evaluate the chemical species present in the surface of the steam-oxidized specimens using X-ray photoelectron spectroscopy.
2. Investigate the crystalline structure of the oxides formed in ATF cladding candidates exposed to steam-environment using X-ray diffraction analysis.
3. Investigate the chemistry and microstructure of the oxides formed in ATF cladding candidates exposed to steam-environment using scanning electron microscopy, transmission electron microscopy, and energy dispersive spectroscopy.

1.3.3 Objective 3: Preliminary determination of mechanical properties of the selected ATF cladding materials

This objective seeks to determine the hardness of the selected cladding materials after oxidation. The hardness of the materials shows how resistant the cladding materials are to wear

in the system and how the materials age under the selected conditions. The hardness of the material is necessary for comparison with irradiation hardening behavior [39].

This final specific objective aims to investigate the changes in the hardness of the as-received and oxidized selected cladding candidates using a set of materials characterization tools.

The tasks followed to complete objective 3 are listed below.

Tasks:

1. Investigate the hardness through micro-indentation of the cross-sections of selected cladding materials before and after steam oxidation.

Chapter 2: Accident Tolerant Fuel Claddings Background and Significance

2.1 Nuclear Reactors

Current nuclear reactor designs being used are primarily generation II light water reactors; with the generation I reactors being early prototype reactors and generation III being advanced light water reactors [40]. Generation II reactors makeup 82% of all reactors in the world and consist of pressurized water reactors (PWR) and boiling water reactors (BWR) [22], [41]. The difference between reactor designs is that PWR designs use pressurized water to cool the reactor core in an indirect cycle, while BWR designs use steam fed in a direct cycle. The steam is used to turn turbines that generate electricity. The indirect cycle is when the coolant is circulated through the core in a single-phase flow and then is fed into a steam generator.

Drawbacks to the PWR and BWR designs include fuel failure where insufficient cooling leads to cladding damage [41], [42]. The reactors that use water as a coolant have the uranium dioxide fuel placed in zirconium alloy claddings within the fuel assembly. While these claddings materials provide excellent performance in normal operating conditions in the reactor, their exposure to high temperatures and steam, typical of accident conditions, leads to hydrogen production and eventually fuel failure.

2.2 Zircaloy-2 and Zircaloy-4

Current commercial fuel claddings used in water-cooled reactors are Zircaloy-2 and Zircaloy-4. Zircaloy alloys are made primarily from zirconium, tin, iron, chromium, and nickel, as provided in table 1.1 [8]. Zircaloy claddings have been the choice of fuel cladding for nuclear reactors since their early development in the 1950s. Zircaloy-2 was originally developed in the early 1950s; the design of Zircaloy-2 was based primarily on zirconium as it has a low neutron absorption cross-section and the ability to withstand high temperatures and pressures; however, it

exhibits low strength properties and corrosive behavior [8], [12], [43]. Although the original development of Zircaloy-2 sought to reduce the impact of corrosion with respect to pure zirconium, Zircaloy-2's poor performance as a fuel cladding was strongly influenced by its corrosion within water and steam environments. The hydrogen pickup was the result of the cladding being in contact with water [8], [12], [43]. Zircaloy-4 is primarily designed as an upgraded form of Zircaloy-2 and is meant to reduce the amount of hydrogen gas produced when the cladding oxidizes. The primary design change between Zircaloy-4 and 2 is the reduction of the content of Nickel and Iron. The increased amount of nickel in the alloy was shown to increase the hydrogen pickup of the cladding [44]. A result of this hydrogen pickup and oxidation effect is poor performance in a loss of coolant accident [7], [8], [43], [45].

2.3 Loss of Coolant Accidents

Loss of coolant accidents (LOCAs) are caused by natural disasters, human errors, part failures, and short-term station blackouts (STSB). These accidents represent a loss in core coolant from either a breach in the coolant system or a core cooling failure. A loss of cooling to the core can result in high-temperature steam being produced and the fuel bundles not being in direct contact with the coolant. The oxidation of the Zircaloy claddings within high-temperature steam environments created by a LOCA results in volatile hydrogen gas. This hydrogen gas led to dangerous conditions and the explosion in the Dai-Chi Nuclear Power plant accident [7]–[9]. This loss of coolant can lead to varying temperature and pressure steam environments. In a loss of coolant accident (LOCA), the Zircaloy claddings start to oxidize, and the zirconium within the cladding produces hydrogen gas, as shown in eq. 1.1.

At the Fukushima Nuclear Power plant in 2011, the Great East Japan Earthquake caused a LOCA which caused the coolant systems to fail, and meltdowns occurred between the multiple

reactors at the site. The primary reactors to suffer hydrogen explosions due to the oxidation of the fuel rod cladding after the coolant water vaporized were reactors 3 and 4; which upon the explosions released large amounts of radioactive materials [7]–[9]. After this accident caused by Zircaloy claddings reactivity, there was a need for cladding materials that can withstand accident conditions for longer times and increase coping time for accident response.

2.4 Accident Tolerant Fuel Claddings

A primary goal of accident tolerant fuel cladding materials after the Dai-chi accident is to limit the adverse oxidation effects from zirconium. These cladding materials are developed to reduce risks with both reactivity-initiated accidents (RIA) and LOCAs [46]. Proposed cladding materials chosen to replace Zircaloy claddings are designed to improve fuel properties, contain contaminants, improve mechanical properties, and reduce negative oxidation effects [47].

Candidates for ATF claddings can be broken into two subsets: surface modified claddings and cladding replacements. Coated claddings offer the convenience of modifying readily available claddings, while cladding replacements allow for improved overall properties [43], [47]–[53].

2.5 FeCrAl Alloys

Compared to traditional Zircaloy claddings, FeCrAl alloys offer improved corrosion resistance, higher coefficients of thermal expansion, and mechanical strength. A key feature of these alloys is the oxidation pattern, which has been widely researched. The oxidation patterns of FeCrAl are temperature-dependent but tend to follow similar processes. First, the structure initially produces a chromium-rich oxide protective layer up to ~1000 °C, followed by aluminum oxide formation as the temperature increases. This oxidation process creates a protective layer of either aluminum or chromium oxides (or a combination) that reduces the degradation of the

substrate. Additionally, the oxidation method reduces the amount of hydrogen gas produced [9], [17]–[23]. Figure 2.1 gives a visual representation of the oxidation process of FeCrAl alloys.

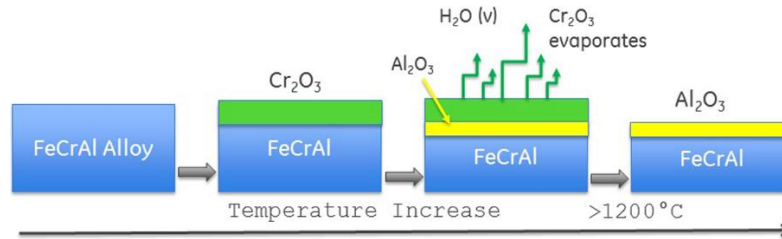


Figure 2.1 Oxidation Behavior of FeCrAl in Super-Heated Steam [9]

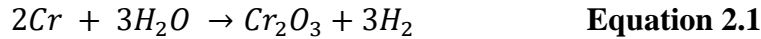
The amount of aluminum and chromium present in the alloy is not paramount to the yield strength, ductility, and radiation resistance at lower temperature ranges, but at higher temperatures, these materials strongly influence these characteristics [54]. The drawbacks related to FeCrAl materials are that the claddings have a higher neutron absorption cross-section, reducing the efficiency of the fuel [54]. Nonetheless, this can be alleviated by reducing the thickness of the tubes, which would also allow for an increase in the fuel pellet volume. Commercially manufactured available FeCrAl alloys include APMT and C26M. C26M is an alloy produced from traditional manufacturing processes of melting materials together [18], [20], [21], [55]. This alloy exhibits improved mechanical properties compared to Zircaloy claddings. These properties are shown in Table 2.1 and show the properties for the C26M.

Table 2.1 Mechanical Properties of C26M [56]

Sample	Hardness (GPa)	Modulus (GPa)
C26M Non-weld Axial	4.43 ± 0.12	236.5 ± 7.11
C26M Non-weld Longitudinal	4.48 ± 0.14	249.2 ± 7.05
C26M Tube Axial	4.13 ± 0.11	227.4 ± 5.94
C26M Tube Longitudinal	4.01 ± 0.14	218.0 ± 7.93

2.6 Chromium-Coated Zirconium alloys

The improvement of current zirconium alloys has led to the development of coated Zircaloy claddings. Coated Zircaloy materials modify currently used commercial nuclear fuel claddings to improve oxidation resistance [25], [47]. The surface materials can be applied through various coating techniques, such as laser coating, cold spraying, and physical vapor deposition (PVD) [43], [47]–[52]. The coatings chosen can be specific metals, alloys, or other materials applied to the surface of the Zircaloy claddings. These coatings are selected to improve the oxidation characteristics while decreasing the impact of the coatings on the neutron absorption cross-section. A primary choice of metal to coat Zircaloy is chromium. Chromium has been a proven coating material because of its oxidation resistance within humid environments, specifically high-temperature steam. The oxidation reaction of the chromium requires more chromium to produce the volatile hydrogen gas compared to the zirconium as shown in equations 1.1 and 2.1 [57].



Chromium's effectiveness as a coating does diminish in extreme temperatures [17], [18], [23], [25], [43], [47]–[51]. Chromium-coated Zircaloy claddings also show improved mechanical properties compared to pure Zircaloy claddings. The hardness and modulus for chromium-coated claddings, Zircaloy-2, and Zircaloy-4 claddings are shown in Table 2.2.

Table 2.2 Mechanical Properties of Chromium-Coated Zircaloy, Zircaloy-2, and Zircaloy-4 [58]

Material	Hardness (GPa)	Modulus (GPa)
Cr Coated	2.85-14.2	140-300
Zr-2	1.8-2.2	95-110
Zr-4	2.0-3.0	99-115

2.7 Steam Oxidation

Loss of coolant accidents creates a high-temperature steam environment in a reactor which rapidly leads to an increase in cladding temperature. To simulate these conditions, the materials are generally exposed for a long term to a high-temperature steam environment to investigate their oxidation behavior and overall performance in the possibility of a loss of coolant accident. One of the current needs in developing accident tolerant fuel cladding materials is their improved reaction kinetics with steam, typically above 400 °C [9]. Oxidation behaviors for FeCrAl and coated Zircaloy-4 cladding materials have been observed for stagnant steam environments within high-temperature ranges. Still, little classification of oxidation has been done for flowing high-temperature steam. [9], [17]–[23]. Table 2.3 summarizes some results from the literature related to high-temperature oxidation of ATF cladding candidate materials.

Table 2.3 Summary of Oxidation Environments and Results

Material	Environment	Time of exposure	Results	Ref.
FeCrAl: C26M and APMT	Flowing air and steam at varying temperatures from 800 °C-1300 °C	2 hours and 4 hours	For C26M: The external layer tended to be distinctively Aluminum followed by an Al-Cr-Fe region	[18]
Zircaloy-4 and FeCrAl alloys	High-temperature water between 290 °C at 7.5 MPa and 330 °C at 15 MPa	0 to 12 months	FeCrAl alloys formed a Cr-rich spinel oxide (chromite) with Fe-rich spinel crystals on its outer surface. The FeCrAl samples resulted in net mass loss	[19]
FeCrAl: C26M	Stagnant air between 300 °C-600 °C	100-2000 hours	The FeCrAl alloy forms an amorphous aluminum oxide and exhibits a lower critical crystalline transition temperature of 500 °C	[20]
Chromium-coated Zircaloy-4	Static water at 360 °C at 18.7 Mpa, Static Steam at 415 °C at 100 bar, and Flowing Steam from 1000 °C-1200 °C	-	Fully formed coatings resulted in a good compromise of increased corrosion resistance and adhesion of the coating, good fretting resistance, and improved resistance to steam oxidation at HT	[25]
Zircaloy-4 and chromium-coated Zircaloy-4	Flowing steam at 500 °C and 1200 °C	0-20 days	The chromium coating resulted in increased resistance to corrosion compared to Zircaloy-4	[26]
Zircaloy-4	Flowing steam at 425 °C, 700 °C, 850 °C, and 950 °C	0-250 days	Pre-oxidized samples (425 °C) developed a thick oxide layer with radial and perpendicular cracks	[59]

Chapter 3: Experimental Procedure

3.1 Materials and Preparation

The materials selected for high-temperature steam oxidation testing are commercially available nuclear grade Zircaloy-4, chromium-coated Zircaloy-4 manufactured by PVD, and FeCrAl alloy C26M, provided by General Electric[®]. The chromium coating was prepared on as-received Zircaloy-4, and the manufacturing process parameters have been described in previous work by the research group [24]. In this study, the samples were half-cylinders cut from commercial tubing. The samples were subjected to humid airflow in the Massachusetts Institute of Technology's Oxidation facility for 20 days [60]. The humid airflow rate was at 2 Standard cubic feet per hour at standard atmospheric pressure and 500 °C, and the testing setup for the oxidation of the sample is shown in figure 3.1.

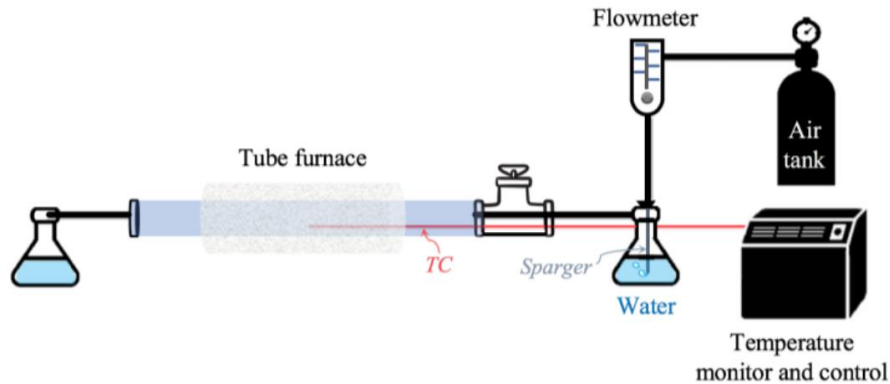


Figure 3.1 Oxidation Testing Facility [60]

Samples were cut for SEM imaging, TEM imaging, XPS, and hardness testing using a Buehler IsoMet Low-speed Precision cutter mounted with a 5-inch CBN/Diamond Hybrid Wafering Blade. For SEM and hardness testing, the samples were cut in 3-5 mm sections and mounted in EpoxyMount Resin. The non-oxidized samples, shown in Figure 3.2, and samples after oxidation, shown in Figure 3.3, evidence their change in surface appearance. The polishing

procedure for the specimens mounted in epoxy resin is shown in Table 3.1. After polishing, the epoxy-mounted samples were cleaned using acetone and an ultrasonic cleaner.

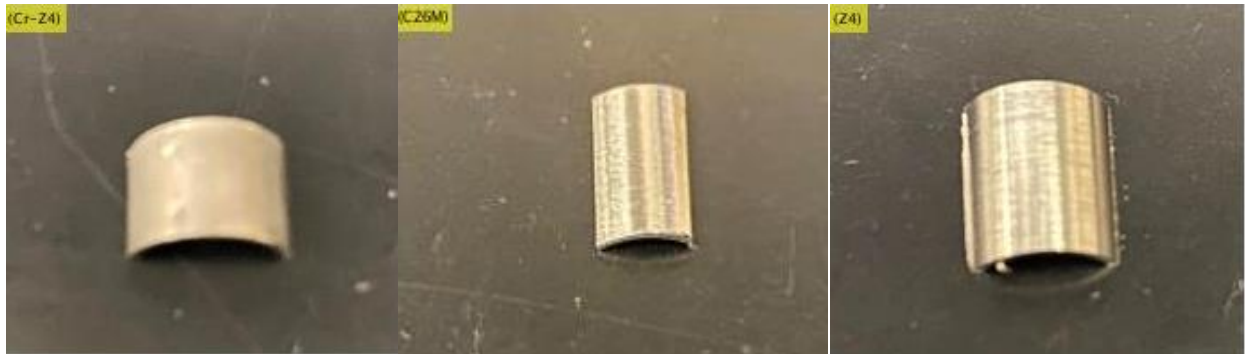


Figure 3.2 Non-Oxidized Cladding



Figure 3.3 Oxidized Samples

Table 3.1 Polishing Procedure

Grit/ Solution	Rotation Direction of Head and Base	Time (min)	Force (lbs)
400 SiC/Water	Together	5	2
600 SiC/Water	Together	5	2
800 SiC/Water	Together	5	2
1200 SiC/Water	Together	5	2
Micro Cloth/ 9um* DIAMAT MA High Viscosity Diamond Suspension	Opposite	5	2
Micro Cloth/ 3um* DIAMAT MA High Viscosity Diamond Suspension	Opposite	5	2

* Between each step the scratch sizes were measured using optical microscopy (Nikon Eclipse LV100D)

3.2 Surface Characterization

The surface topography and wettability of the sample were characterized through surface roughness measurements, following American Society of Testing Materials (ASTM) standards, and static contact angle measurements, following International Organization for Standardization (ISO) standards [61]–[65]. The Mitutoyo SurfTest SJ-410 was used for the surface roughness profile. The device scanned the surface for Ra, Rq, Rz, and Rsm values using a scan distance of 1 mm at 0.1 mm/s with a 0.8 mm gauss filter. The specific surface characteristics chosen were: Ra, is the roughness average, Rq, is the root mean square roughness, Rz, is the average maximum height of profile, and Rsm is the spacing of irregularities [66]. The samples were placed on carbon tape on a microscope slide for surface roughness testing to avoid the sample from sliding on the leveling surface, and sets of 10 data points were collected. The slides were taped to the leveling plate of the Mitutoyo SurfTest SJ-410, as shown in Figure 3.4. The

material's surface was then made level to the tester through the contact of the stylus at both the leading and furthest edge.

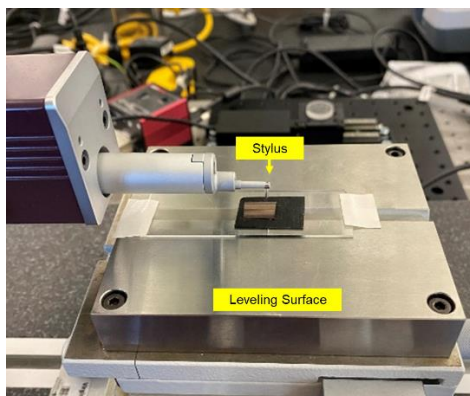


Figure 3.4 Mitutoyo Surftest SJ-410 Testing Setup

The static contact angle of the surface was determined using a Rame-Hart Contact Angle. Multiple measurements were taken by depositing a 2 μL droplet on the surface with 20 data points over a 1-second duration. This process was repeated for all the oxidized samples. Figure 3.5 shows the landed droplet on the level sample for the testing setup.

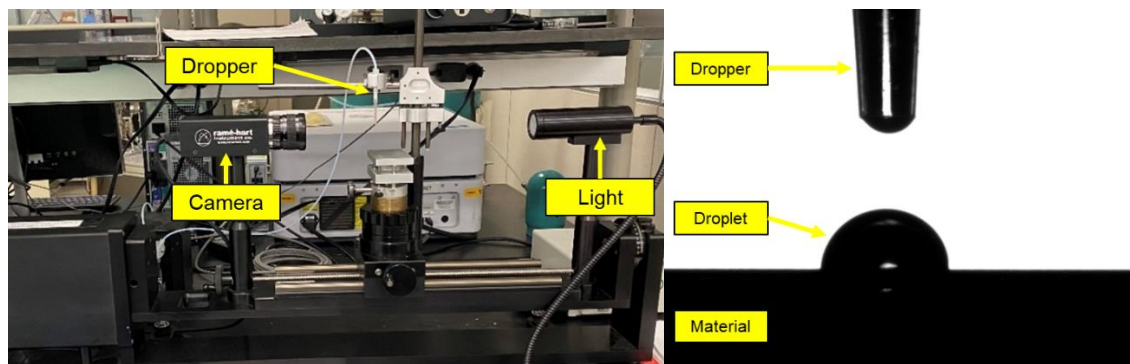


Figure 3.5 Rame-Hart Contact Angle Testing Setup and Landed Drop

3.3 Surface Chemistry and Microstructure

The samples were imaged using a Phenom ProX SEM. The samples were also analyzed for chemical composition using EDS and element identification. The SEM operated at a voltage

of 10 kV for imaging and 15 kV for EDS. The samples were imaged to determine the thickness of the oxide layers and composition. TEM imaging and analysis were conducted at the University of Virginia using a FEI Titan and a Themis 60-300 kV Transmission Electron Microscopes. The samples were cut and welded to a copper grid using a focused ion beam. The samples were then imaged, and the chemical composition was characterized using EDS and element identification.

XRD was used to identify changes in the material's crystalline structure and the nature of the oxides formed on their surface. The samples were placed onto an aluminum disk mounted on the chi-x stage in the Empyrean Multipurpose X-ray Diffractometer equipped with a Copper target (voltage 45 kV, current 40 mA, and $\lambda K\alpha_1 = 1.5406 \text{ \AA}$). The samples were analyzed using a step size of $0.0070^\circ 2\theta$, starting at 30 degrees, and a step time of 78.7950 seconds.

XPS measurements were taken on the samples using the PHI VersaProbe III Scanning XPS Microprobe, equipped with a monochromated Al k-Alpha X-ray source. Depth profiling and high-resolution scans were conducted for each sample. A standard SiO_2 specimen was observed for depth profiling measurements for calibration, and the depth profiling procedure is shown in Table 3.2. The depth profiling of the SiO_2 sample showed there was roughly a 1.67 nm/min etching rate. The scanning procedures for the oxidized samples are shown in Tables 3.3-3.5.

Table 3.2 SiO₂ Scanning Procedure

Material	SiO₂	
Scan Type	Number of Cycles	Cycle Time (min)
High Resolution	1	1
Depth Profile	3	1
Depth Profile	5	1
Depth Profile	5	1
Depth Profile	5	1
High Resolution	1	1

Table 3.3 C26M Scanning Procedure

Material	C26M	
Scan Type	Number of Cycles	Cycle Time (min)
Depth Profile	1	2
High Resolution	1	13
Depth Profile	2	2
High Resolution	1	13
Depth Profile	3	2
High Resolution	1	13
Depth Profile	5	2
High Resolution	1	13
Depth Profile	5	2
High Resolution	1	13
Depth Profile	10	2
High Resolution	1	13

Table 3.4 Chromium-Coated Zircaloy-4 Scanning Procedure

Material	Chromium-Coated Zircaloy-4	
Scan Type	Number of Cycles	Cycle Time (min)
Depth Profile	1	2
High Resolution	1	13
Depth Profile	2	2
High Resolution	1	13
Depth Profile	3	2
High Resolution	1	13
Depth Profile	5	2
High Resolution	1	13
Depth Profile	5	2
High Resolution	1	13
Depth Profile	5	2
High Resolution	1	13
Depth Profile	10	2
High Resolution	1	13
Depth Profile	12	2
High Resolution	1	13

Table 3.5 Zircaloy-4 Scanning Procedure

Material	Zircaloy-4	
Scan Type	Number of Cycles	Cycle Time (min)
Depth Profile	1	2
High Resolution	1	13
Depth Profile	2	2
High Resolution	1	13
Depth Profile	3	2
High Resolution	1	13
Depth Profile	5	2
High Resolution	1	13
Depth Profile	5	2
High Resolution	1	13
Depth Profile	5	2
High Resolution	1	13
Depth Profile	10	2
High Resolution	1	13

3.4 Mechanical Testing

The samples mounted in epoxy for hardness testing were polished on both the top and bottom surfaces. The samples were ground and polished on both sides to ensure the metal was exposed and in contact with the mount and tester. The samples were placed top-up in the mount for the Bruker TUKON-1202 micro-hardness tester. These samples were subjected to an applied load of 25 gram-force for 15 seconds.

Chapter 4: Results and Discussion

4.1 Surface Roughness and Wettability

The average surface roughness and contact angle measurements of the oxidized and as-received samples are shown in Table 4.1. Specifically, the oxidized samples showed the variation with the as-received samples in the Rsm values, which represented a wider distance between irregularities; the percentage increases of the Rsm values are 40% for C26M, 17% for chromium-coated Zircaloy-4, and 14% for Zircaloy-4. In general, oxidized cladding materials showed an increase in roughness values compared to the as-received samples. The Zircaloy-4 and FeCrAl materials became more hydrophobic after oxidation. Chromium-coated Zircaloy did not change after oxidation compared to the as-received samples.

The slight increase in roughness parameters may be attributed to the oxide formation in the samples from exposure to the high-temperature steam environment. The increase in surface roughness has also been reported in previous work on these accident tolerant fuel materials after critical heat flux testing at ambient pressure [24], [67]. The contact angles for C26M and Zircaloy-4 showed an increase and became less hydrophilic. This increase in contact angle for C26M is the opposite of what has been reported in previous work after critical heat flux testing at ambient pressure [67]. Similarly, the contact angle for chromium-coated Zircaloy-4 remaining unchanged does not agree with what has been reported in previous work after critical heat flux testing at ambient pressure, where the contact angle increased [24].

Table 4.1 Roughness and Contact Angle Comparison Between As-Received and Oxidized Samples

Sample		Roughness Parameters				Contact Angle (degrees)
		Ra (μm)	Rq	Rz (μm)	Rsm (μm)	
C26M	As-Received	0.631 \pm 0.028	0.818 \pm 0.028	5.195 \pm 0.28	97.56 \pm 13.039	77.70 \pm 0.28
	Oxidized	0.698 \pm 0.029	0.923 \pm 0.032	8.451 \pm 0.743	137.493 \pm 16.9	87.73 \pm 1.45
Zr4	As-Received	0.434 \pm 0.058	0.547 \pm 0.075	4.032 \pm 0.693	66.936 \pm 6.1	75.42 \pm 3.21
	Oxidized	0.427 \pm 0.053	0.551 \pm 0.063	4.363 \pm 0.523	76.84 \pm 9.3	80.53 \pm 4.73
Zr4-Cr	As-Received	0.455 \pm 0.06	0.578 \pm 0.076	4.315 \pm 0.8	71.728 \pm 7	91.95 \pm 7.28
	Oxidized	0.45 \pm 0.068	0.603 \pm 0.088	5.361 \pm 0.784	84.527 \pm 6.9	89.31 \pm 0.05

4.2 Surface Chemistry

Figure 4.1 shows the SEM images of the cross-sections and oxide layers of the oxidized C26M, chromium-coated Zircaloy-4, and Zircaloy-4 samples. The chromium layer of the coated Zircaloy sample is easily visible and measured using ImageJ to be between 5 and 7 μm thick. The oxidation of the chromium-coated Zircaloy-4 can be seen at the surface and in the crevices in the chromium layer. Additionally, the oxide layer of the Zircaloy-4 is evident and was measured to be \sim 20 μm thick. Due to the thick oxide layer of the Zircaloy-4, the material became highly brittle, and the cracks in the oxide layer are visible in Figure 4.1 c.

The diffraction patterns shown in Figure 4.2 show a body-centered cubic (BCC) structure for C26M, and a hexagonal closed packed (HCP) structure for the Zircaloy-4 [8], [24], [68], [69]. The crystalline structure has also been reported in previous work on these accident tolerant fuel materials after critical heat flux testing at ambient pressure [24], [67].

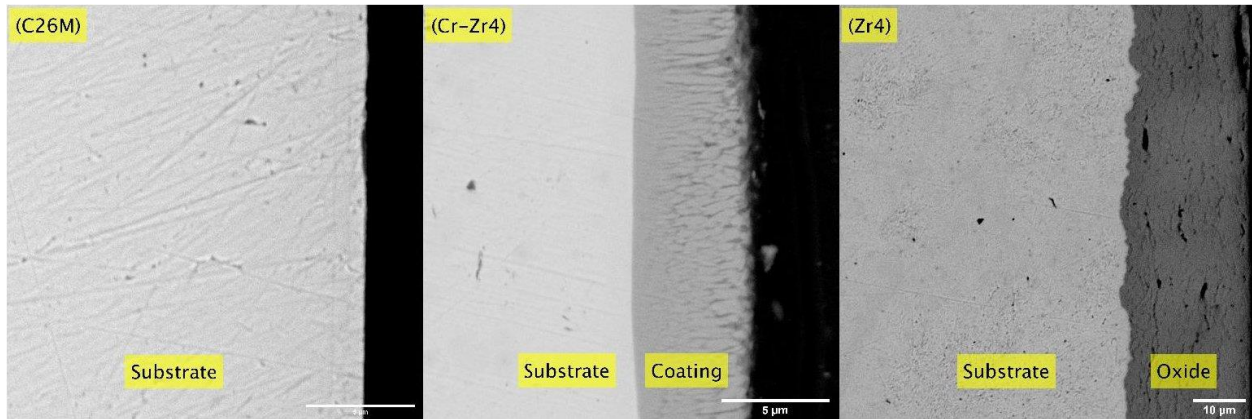


Figure 4.1 SEM images of the cross-sections and oxide layers of selected cladding materials

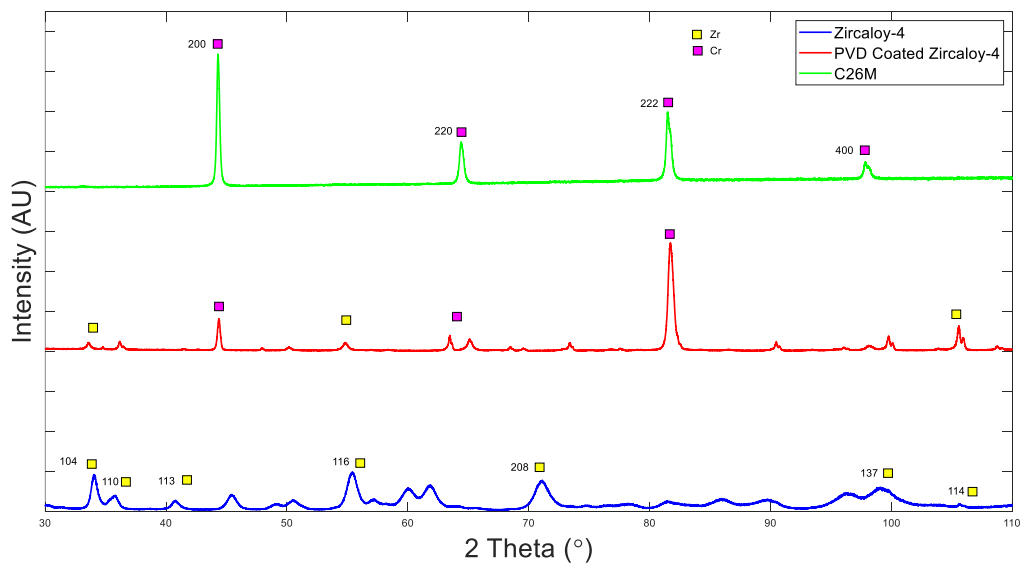


Figure 4.2 XRD Patterns for oxidized Zircaloy-4, chromium-coated Zircaloy-4, and C26M

The XPS depth profiles for all materials shown in Figure 4.3 show an oxygen content until the end of sputtering. For all profiles, the thickness of oxides is difficult to quantify due to the varying material nature; therefore, all results for XPS depth profiling are presented in terms of sputtering time. The determination of depth profiling in terms of sputtering time is

documented in previous work for these materials after critical heat flux testing at ambient pressure [67].

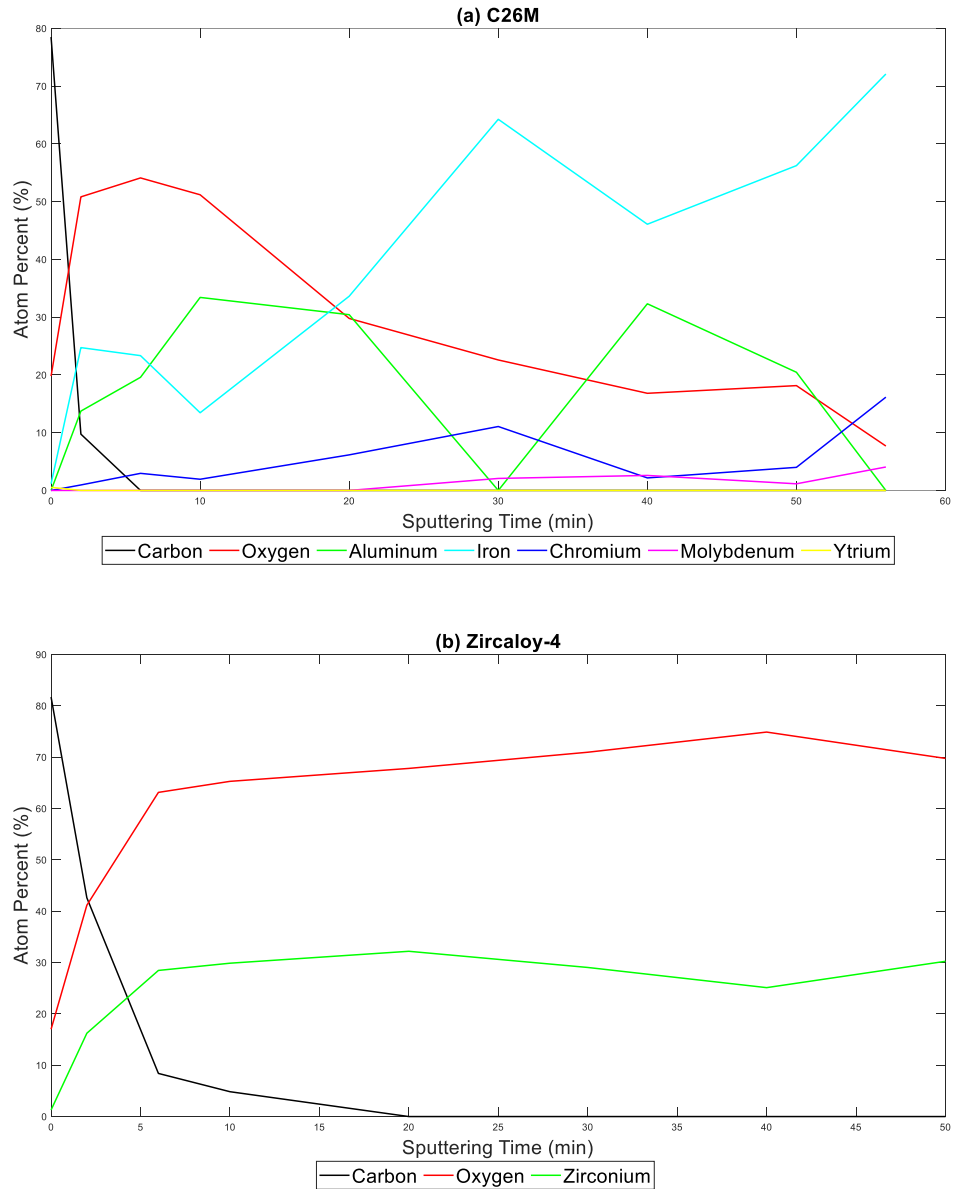


Figure 4.3 Element composition vs. Depth profile (sputter time) on the Oxidized Samples: (a) C26M (b) Zircaloy-4 (c) chromium-coated Zircaloy-4 with accompanying high-resolution scan at 20 minutes

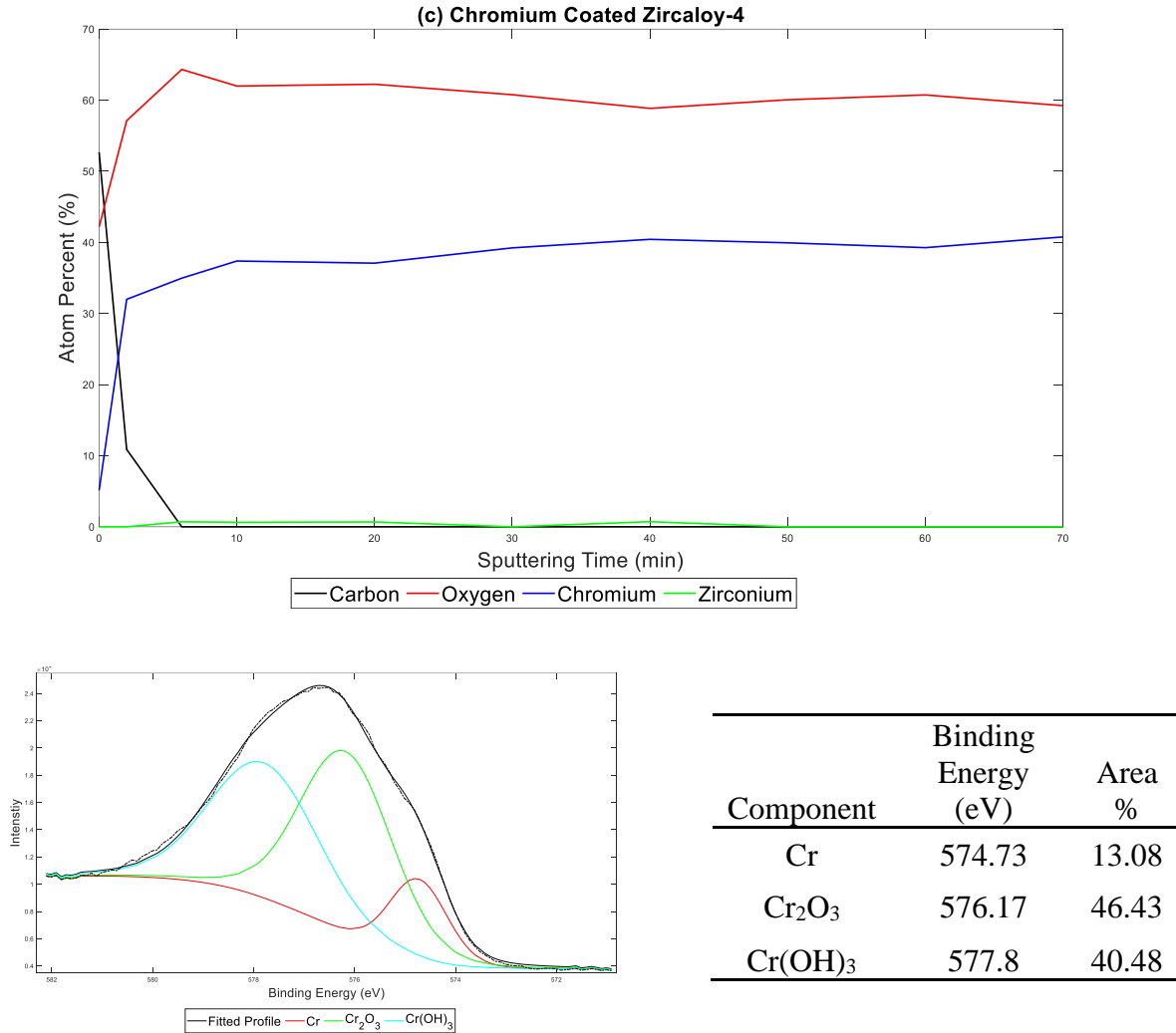


Figure 4.3 (cont.) Element composition vs. Depth profile (sputter time) on the Oxidized Samples: (a) C26M (b) Zircaloy-4 (c) chromium-coated Zircaloy-4 with accompanying high-resolution spectra at 20 minutes

The XPS depth profiling shown in Figure 4.3a shows a large iron content at the surface oxide layer, up to 7 minutes of sputtering, followed by an internal oxide layer rich in aluminum. Below the aluminum oxide, a mix of iron, chromium, and aluminum corresponds to the substrate material. The oxide layer for C26M can be seen in the STEM images in Figure 4.4a and visually shows what is described by XPS. The images evidence an external layer rich in iron with a low content of aluminum and chromium. In addition, there is an internal oxide layer that is rich in aluminum. The oxide layer is around 150nm in Figure 4.4 a. The oxidation behavior of FeCrAl

cladding materials tends to have a chromium and aluminum oxide layer that forms to create a protective coating. Still, the tested material has an increased iron content at the surface. The mixed oxides at the material's surface have been reported in temperature ranges below 950 °C. Additionally, the high iron content observed at the surface has been reported to develop in air oxidation at 500 °C [18]–[20].

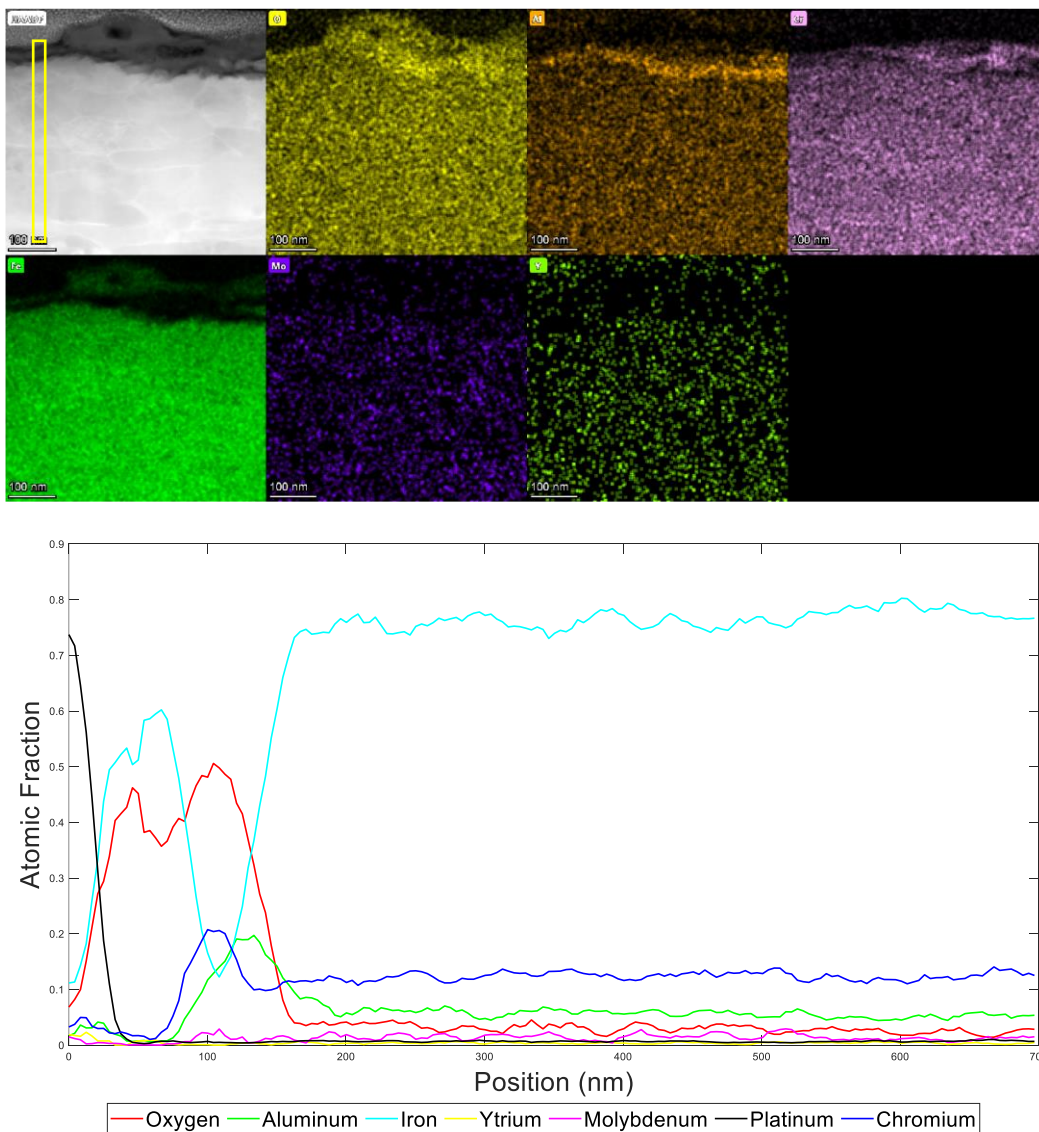


Figure 4.4 TEM observation of C26M: (a) STEM image of the oxide layer formed on C26M with associated EDS chemical maps (b) EDS line scan across the oxide layer

Chromium oxide is shown to extend to the end of sputtering in the XPS depth profiling for the chromium-coated Zircaloy-4 shown in Figure 4.3c. Additionally, the deconvolution of the high-resolution spectra at 20 minutes in Figure 4.3c shows the majority of the chromium is oxidized into chromium oxide (Cr_2O_3) and chromium hydroxide ($\text{Cr}(\text{OH})_3$). The oxide layer for chromium-coated Zircaloy-4 can be seen in the EDS map in Figure 4.5a. The roughness values for the chromium-coated Zircaloy-4 shown in Table 4.1 cause the peaks and valleys to be increasingly visible, as shown in Figure 4.1b and Figure 4.5a where the coating process has generated large crevices. The oxidation layer is shown in Figure 4.5a and is shown to react heavily in the crevices created by the coating. The highest intensity oxide layer shown through TEM is roughly $0.5 \mu\text{m}$ deep in Figure 4.6b. Still, the oxide penetration can be seen in Figure 4.5a to follow the crevices to the edge of the chromium and zirconium substrate, although there is little to no oxide shown in the substrate. The growth of the oxide layer follows similar growth patterns to those shown by J. Brachet et al. for samples oxidized in high-temperature steam of $415 \text{ }^\circ\text{C}$ at 100 bar, but the flowing steam results show increased oxygen penetration in the crevices of the coating and increased chromium oxide thickness layer [25].

It is important to note that although the Cr-coating evidenced crevices, the oxygen did not penetrate the point of reaching the Zircaloy substrate. This evidences the protective behavior of the coating at the tested conditions.

Zirconium oxide is shown to extend to the end of sputtering in the XPS depth profiling for the Zircaloy-4 shown in Figure 4.3b. The oxide layer for the Zircaloy-4 sample can be seen in the EDS map in Figure 4.6a and shows large cavities created by the brittleness of the oxide layer. The oxidation shown in Figure 4.6a represents a large portion of the Zircaloy-4 oxidizing, and

the oxide penetration of Zircaloy-4 is shown in Figure 4.6 b. The oxide that can be visually seen in Figure 4.1c was measured using ImageJ and determined to be around 23 μm deep. The results are similar to the results reported by C. Duriez et al. for a 425 $^{\circ}\text{C}$ environment of flowing steam, where radial cracks develop and perpendicular cracks develop in the Zircaloy-4 oxide layer due to the tensile stress caused by the convexity and strain of the substrate and the depth of the oxide layer for samples oxidized for 256 days, was approximately 32 μm [59].

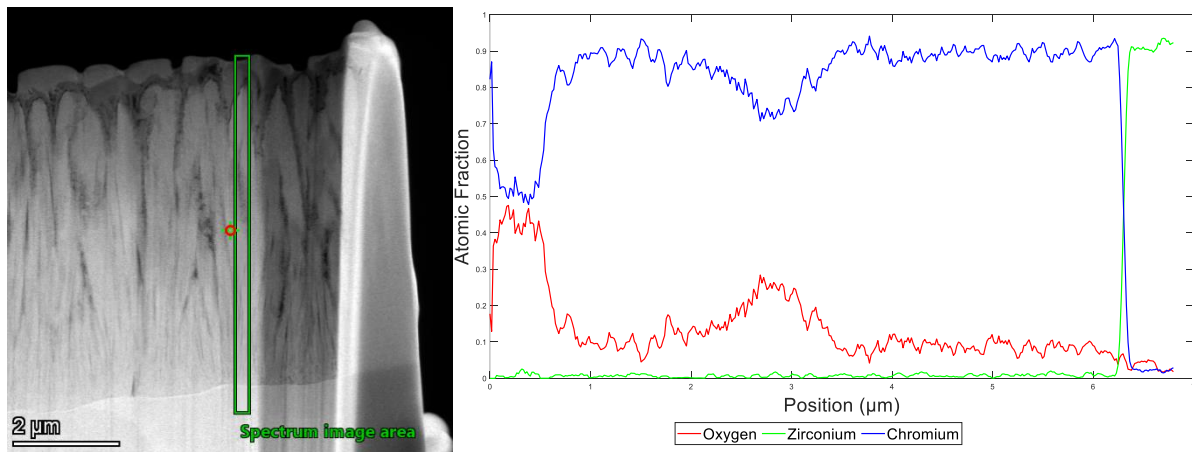
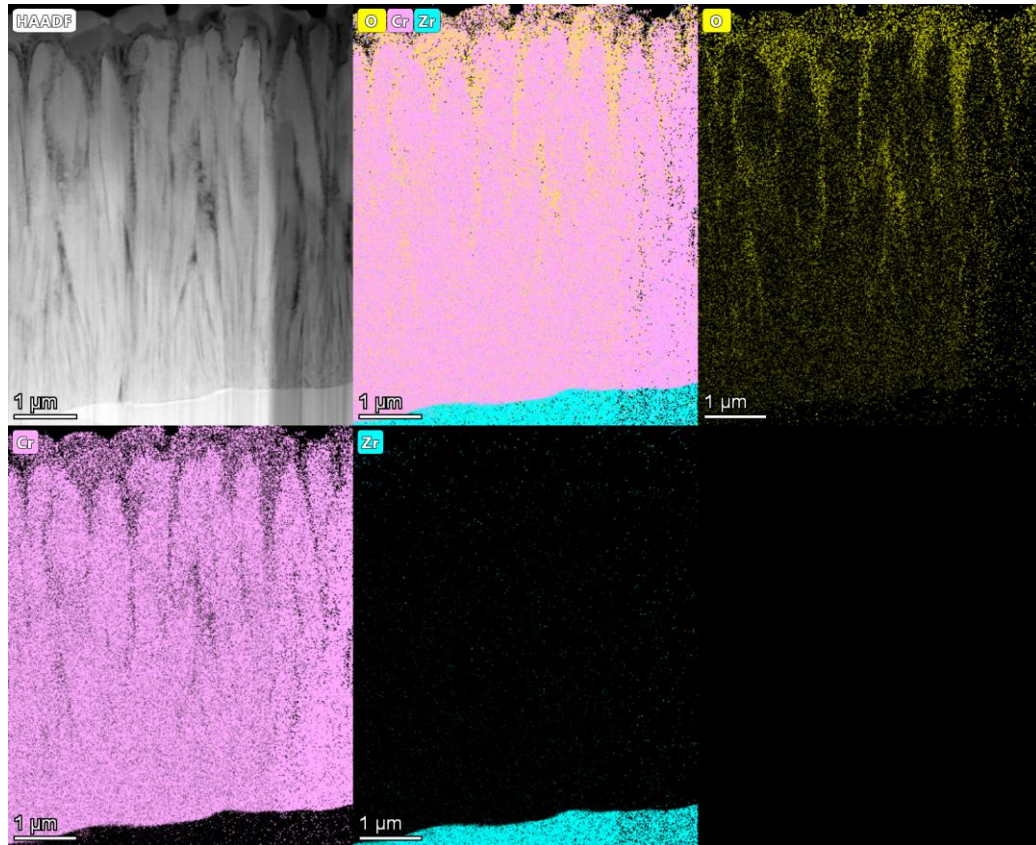


Figure 4.5 TEM observation of chromium-coated Zircaloy-4: (a) STEM image of the oxide layer formed on chromium-coated Zircaloy-4 with associated EDS chemical maps (b) STEM image with associated EDS line scan across the oxide layer

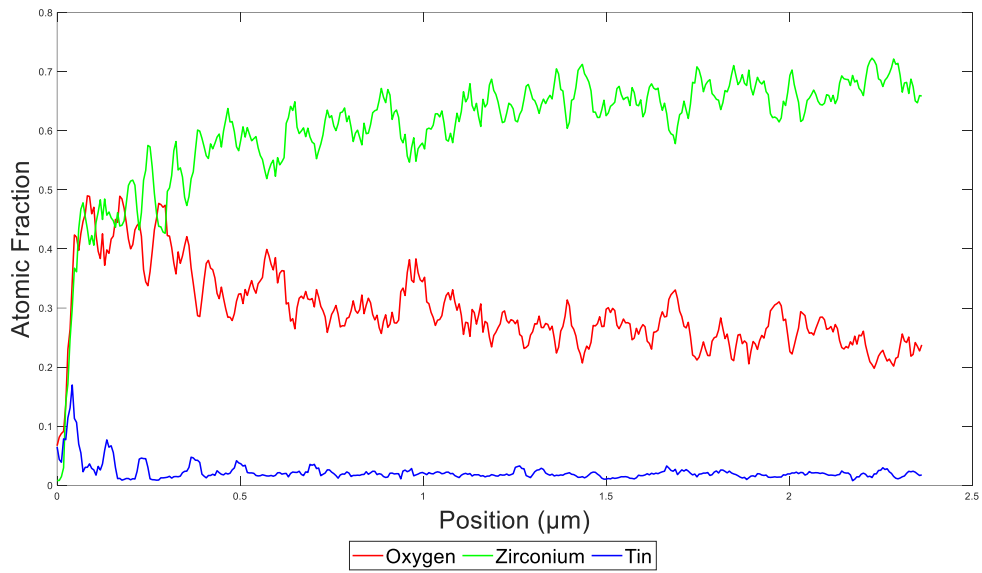
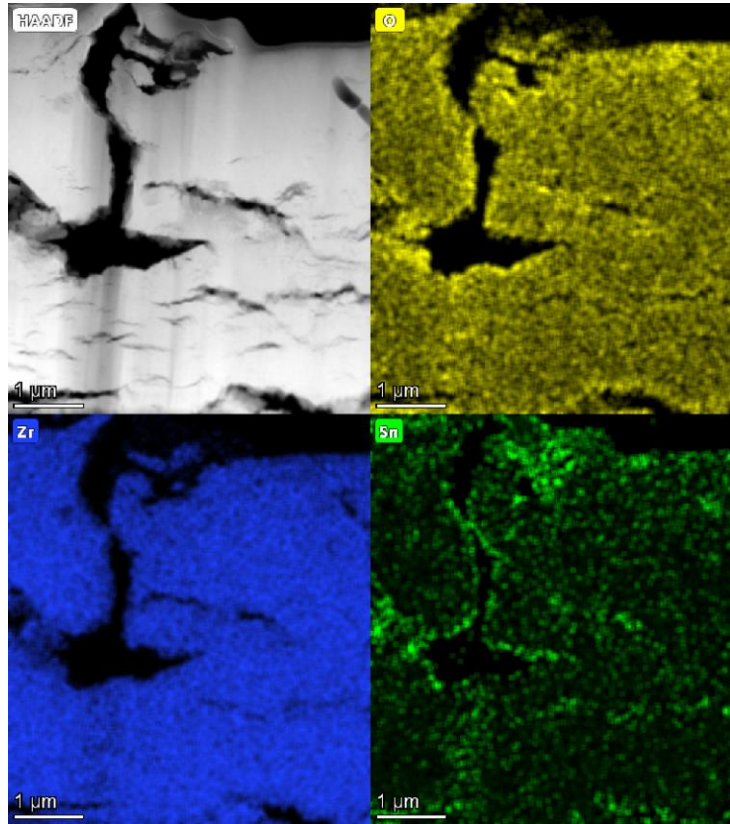


Figure 4.6 TEM observation of Zircaloy-4: (a) STEM image of the oxide layer formed on chromium-coated Zircaloy-4 with associated EDS chemical maps (b) EDS line scan across the oxide layer

In summary, the FeCrAl sample exhibited similar oxidation characteristics to materials oxidized in super-heated environments and liquid environments. The long-term exposure of this material in the high-temperature steam environment evidenced an external oxide layer rich in iron with some a fraction of aluminum and chromium, and an internal layer rich in aluminum. The iron deposits at the surface of C26M correlate with published data from uniform corrosion of FeCrAl alloys in LWR coolant environments at high temperatures [19]. Similarly, the chromium coating on the Zircaloy-4 reduced the impact of oxidation on the substrate [9], [17]–[23].

4.3 Mechanical Properties

The hardness values in Table 4.2 compare the hardness of the as-received samples to the oxidized samples and represent the embrittlement of the surface of the material through oxidation. All observed materials showed a decrease in hardness compared to the received samples and literature values shown in Tables 2.2 and 2.3.

The large decrease in hardness may be attributed to the oxide formation in the samples from exposure to the high-temperature steam environment. The decrease in hardness contrasts observations in previous work on these accident tolerant fuel materials after critical heat flux testing at ambient pressure showed an increase in hardness [24], [67].

Table 4.2 Hardness Comparison for As-Received and Oxidized samples

Sample	Hardness (GPa)
C26M	As-Received 2.408±0.216
	Oxidized 2.300±0.061
Zr4	As-Received 2.241±0.254
	Oxidized 1.789±0.120
Zr4-Cr	As-Received 4.107±0.626
	Oxidized 1.727±0.133

Chapter 5: Conclusions and Future Works

Surface characterization was performed on extended high-temperature, flowing steam oxidized ATF cladding material candidates, including chromium-coated Zircaloy and C26M FeCrAl alloy, compared to Zircaloy-4. The surface properties were characterized by the static contact angle, surface roughness, surface chemistry and microstructure, and mechanical properties. The surface chemistry of the C26M samples revealed an external layer rich in iron, chromium, and aluminum oxide layer below it. The chromium within the coated sample was found to oxidize to some extent. The oxidation of the chromium increased the cavities resulting from the PVD coating but did not result in the coating separating from the Zircaloy-4 substrate. Additionally, the chromium coating prevented the oxidation of the zirconium substrate. All materials were found to reduce their hardness values after high-temperature steam oxidation compared to the received values. The foundation for future studies should be on the impact of surface characteristics on ATF and their impact on their performance with oxidation and heat transfer. Future studies on the impact of steam flow rates on the oxide layer growth and cladding performance should be conducted.

References

- [1] I. Hore-Lacy, *Mankind Benefits From Nuclear Energy and Radiation*, vol. 4. Elsevier, 2021.
- [2] D. B. Adler, A. Jha, and E. Severnini, “Considering the nuclear option: Hidden benefits and social costs of nuclear power in the U.S. since 1970,” *Resour. Energy Econ.*, vol. 59, no. 2020, p. 101127, 2020, doi: 10.1016/j.reseneeco.2019.101127.
- [3] J. Harris, M. Hassall, G. Muriuki, C. Warnaar-Notschaele, E. McFarland, and P. Ashworth, “The demographics of nuclear power: Comparing nuclear experts’ scientists’ and non-science professionals’ views of risks, benefits and values,” *Energy Res. Soc. Sci.*, vol. 46, no. September 2017, pp. 29–39, 2018, doi: 10.1016/j.erss.2018.05.035.
- [4] M. Neidell, S. Uchida, and M. Veronesi, “The unintended effects from halting nuclear power production: Evidence from Fukushima Daiichi accident,” *J. Health Econ.*, vol. 79, no. November 2020, p. 102507, 2021, doi: 10.1016/j.jhealeco.2021.102507.
- [5] J. M. Allan *et al.*, “Investigation into the 03-28-1979 TMI Accident by the Office of IE,” 1979.
- [6] N. J. McCormick, “Changes in the nuclear power industry after TMI,” *Prog. Nucl. Energy*, vol. 10, no. 3, pp. 245–248, 1982, doi: 10.1016/0149-1970(82)90007-5.
- [7] International Atomic Energy Agency, “Expert Mission Iaea International Fact Finding Expert Mission of the Fukushima Dai-Ichi Npp Accident Following the Great East Japan,” *IAEA Int. Fact Find. Expert Mission Fukushima Dai-Ichi NPP Accid. Follow. Gt. East Japan Earthq. Tsunami*, no. June, p. IAEA MISSION REPORT, 2011.

- [8] C. L. Withmarsh, "Review of Zircaloy-2 and Zircaloy-4 Properties Relevant to N.S. Savannah Reactor Design," (*No. ORNL-3281*). *Oak Ridge National Lab., Tenn.*, vol. 4500. p. 70, 1962.
- [9] R. B. Rebak, "Iron-chrome-aluminum alloy cladding for increasing safety in nuclear power plants," *EPJ Nucl. Sci. Technol.*, vol. 3, p. 34, 2017, doi: 10.1051/epjn/2017029.
- [10] M. C. Billone, H. M. Chung, and Y. Yan, "Steam Oxidation Kinetics of Zirconium Alloys," 2002.
- [11] R. E. Pawel, J. V. Csthart, J. J. Campbell, and S. H. Jury, "Zirconium Metal-Water Oxidation Kinetics V. Oxidation of Zircaloy in High Pressure Steam," *Ornl/Nureg-31*, *Ornl*, 1977.
- [12] D. E. Thomas and F. Forscher, "Properties of Zircaloy-2," pp. 2–29, 1955.
- [13] P. B. Scott, "Physical and Mechanical Properties of Zircaloy -2 and -4," *Wcap*, vol. 3269, pp. 3269–41, 1965.
- [14] ATI Metals, "Zircaloy-4 Annealed - Technical Data Sheet," vol. 1, pp. 2014–2016, 2015, [Online]. Available:
https://www.atimetals.com/Products/Documents/datasheets/zirconium/alloy/Zr_nuke_was_te_disposal_v2.pdf.
- [15] "Department of Energy." <https://www.energy.gov/> (accessed Nov. 22, 2021).
- [16] "Accident Tolerant Fuel | NRC.gov." <https://www.nrc.gov/reactors/atf.html> (accessed Nov. 15, 2021).
- [17] L. J. Ott, M. Howell, and K. R. Robb, *Parametric and experimentally informed BWR*

- Severe Accident Analysis Utilizing FeCrAl - M3FT-17OR020205041*, no. August. 2017.
- [18] R. B. Rebak, V. K. Gupta, and M. Larsen, "Oxidation Characteristics of Two FeCrAl Alloys in Air and Steam from 800°C to 1300°C," *JOM*, vol. 70, no. 8, pp. 1484–1492, Aug. 2018, doi: 10.1007/s11837-018-2979-9.
- [19] K. A. Terrani *et al.*, "Uniform corrosion of FeCrAl alloys in LWR coolant environments," *J. Nucl. Mater.*, vol. 479, pp. 36–47, 2016, doi: 10.1016/j.jnucmat.2016.06.047.
- [20] N. Li, S. S. Parker, T. A. Saleh, S. A. Maloy, and A. Nelson, "Intermediate Temperature corrosion behavior of Fe-12Cr-6Al-2Mo-0.2Si-0.03Y alloy (C26M) at 300-600 C," 2019.
- [21] R. B. Rebak, "Beneficial Oxidation Resistance of FeCrAl Alloys for Accident Tolerant Fuel Cladding," no. March, pp. 1–8, 2011.
- [22] E. Dolley *et al.*, "Development of LWR Fuels with Enhanced Accident Tolerance," *J. Nucl. Mater.*, vol. 448, no. 1–3, p. 327, 2014, doi: 10.1016/j.jnucmat.2013.09.052.
- [23] H. Ebrahimgol, M. Aghaie, and A. Zolfaghari, "Evaluation of ATFs in core degradation of a PWR in unmitigated SBLOCA," *Ann. Nucl. Energy*, vol. 152, p. 107961, 2021, doi: 10.1016/j.anucene.2020.107961.
- [24] R. V. Umretiya, B. Elward, D. Lee, M. Anderson, R. B. Rebak, and J. V. Rojas, "Mechanical and chemical properties of PVD and cold spray Cr-coatings on Zircaloy-4," *J. Nucl. Mater.*, vol. 541, p. 152420, Dec. 2020, doi: 10.1016/j.jnucmat.2020.152420.
- [25] J. C. Brachet *et al.*, "Early studies on Cr-Coated Zircaloy-4 as enhanced accident tolerant nuclear fuel claddings for light water reactors," *J. Nucl. Mater.*, vol. 517, pp. 268–285, Apr. 2019, doi: 10.1016/j.jnucmat.2019.02.018.

- [26] M. Ševeček *et al.*, “Development of Cr cold spray–coated fuel cladding with enhanced accident tolerance,” *Nucl. Eng. Technol.*, vol. 50, no. 2, pp. 229–236, Mar. 2018, doi: 10.1016/j.net.2017.12.011.
- [27] D. Lee *et al.*, “Enhanced flow boiling heat transfer on chromium coated zircaloy-4 using cold spray technique for accident tolerant fuel (ATF) materials,” *Appl. Therm. Eng.*, vol. 185, Feb. 2021, doi: 10.1016/j.applthermaleng.2020.116347.
- [28] P. Platt, V. Allen, M. Fenwick, M. Gass, and M. Preuss, “Observation of the effect of surface roughness on the oxidation of Zircaloy-4,” *Corros. Sci.*, vol. 98, pp. 1–5, 2015, doi: 10.1016/j.corsci.2015.05.013.
- [29] H. F. O’Hanley, “Separate Effects of Surface Roughness, Wettability and Porosity on Boiling Heat Transfer and Critical Heat Flux and Optimization of Boiling Surfaces,” pp. 1–45, 2013.
- [30] K.-Y. Law, “Definitions for Hydrophilicity, Hydrophobicity, and Superhydrophobicity: Getting the Basics Right,” *J. Phys. Chem. Lett.*, vol. 5, no. 4, pp. 686–688, 2014.
- [31] A. F. Ali *et al.*, “Surface wettability and pool boiling Critical Heat Flux of Accident Tolerant Fuel cladding-FeCrAl alloys,” *Nucl. Eng. Des.*, vol. 338, no. April, pp. 218–231, 2018, doi: 10.1016/j.nucengdes.2018.08.024.
- [32] T. Note, “AT-TN-07-Surface-roughness-CA-wettability,” pp. 1–3, 1936.
- [33] A. Marmur, “Solid-surface characterization by wetting,” *Annu. Rev. Mater. Res.*, vol. 39, pp. 473–489, 2009, doi: 10.1146/annurev.matsci.38.060407.132425.
- [34] S. Agarwal, “Engineering Chemistry,” *Eng. Chem.*, pp. 988–994, 2015, doi:

10.1017/cbo9781316146743.

- [35] N. Li, S. S. Parker, E. S. Wood, and A. T. Nelson, “Oxide Morphology of a FeCrAl Alloy, Kanthal APMT, Following Extended Aging in Air at 300 °C to 600 °C,” *Metall. Mater. Trans. A Phys. Metall. Mater. Sci.*, vol. 49, no. 7, pp. 2940–2950, 2018, doi: 10.1007/s11661-018-4649-5.
- [36] H. Ebrahimgol, M. Aghaie, and A. Zolfaghari, “Evaluation of ATFs in core degradation of a PWR in unmitigated SBLOCA,” *Ann. Nucl. Energy*, vol. 152, p. 107961, 2021, doi: 10.1016/j.anucene.2020.107961.
- [37] H. Chen, X. Wang, and R. Zhang, “Application and development progress of Cr-based surface coating in nuclear fuel elements: II. Current status and shortcomings of performance studies,” *Coatings*, vol. 10, no. 9, 2020, doi: 10.3390/coatings10090835.
- [38] Q. Chen *et al.*, “Microstructure evolution and adhesion properties of thick Cr coatings under different thermal shock temperatures,” *Surf. Coatings Technol.*, vol. 417, Jul. 2021, doi: 10.1016/j.surfcoat.2021.127224.
- [39] J. Gigax, A. J. Torrez, and N. Li, “Microstructural and Micromechanical Characterization of FeCrAl C26M tubes,” *United States N. p.*, 2019.
- [40] S. M. Goldberg and R. Rosner, *Nuclear Reactors: Generation to Generation US Department of States*. Cambridge MA: AMERICAN ACADEMY OF ARTS & SCIENCES.
- [41] M. Ho, E. Obbard, P. A. Burr, and G. Yeoh, “A review on the development of nuclear power reactors,” *Energy Procedia*, vol. 160, no. 2018, pp. 459–466, 2019, doi:

10.1016/j.egypro.2019.02.193.

- [42] Y. Oka, H. Madarame, and M. Uesaka, Eds., *Nuclear reactor designs*, vol. 58, no. 25. Ohmsha LTD, 1980.
- [43] C. Tang, M. Stueber, H. J. Seifert, and M. Steinbrueck, “Protective coatings on zirconium-based alloys as accident-Tolerant fuel (ATF) claddings,” *Corros. Rev.*, vol. 35, no. 3, pp. 141–165, 2017, doi: 10.1515/corrrev-2017-0010.
- [44] Y. R. Than, R. W. Grimes, B. D. C. Bell, and M. R. Wenman, “Understanding the role of Fe, Cr and Ni in Zircaloy-2 with special focus on the role of Ni on hydrogen pickup,” *J. Nucl. Mater.*, vol. 530, p. 151956, 2020, doi: 10.1016/j.jnucmat.2019.151956.
- [45] S. Leistikow and G. Schanz, “Oxidation kinetics and related phenomena of zircaloy-4 fuel cladding exposed to high temperature steam and hydrogen-steam mixtures under PWR accident conditions,” *Nucl. Eng. Des.*, vol. 103, no. 1, pp. 65–84, 1987, doi: 10.1016/0029-5493(87)90286-X.
- [46] S. J. Zinkle and G. S. Was, “Materials challenges in nuclear energy,” *Acta Mater.*, vol. 61, no. 3, pp. 735–758, 2013, doi: 10.1016/j.actamat.2012.11.004.
- [47] K. A. Terrani, “Accident tolerant fuel cladding development: Promise, status, and challenges,” *J. Nucl. Mater.*, vol. 501, pp. 13–30, 2018, doi: 10.1016/j.jnucmat.2017.12.043.
- [48] L. D’Avico, R. Beltrami, N. Lecis, and S. P. Trasatti, “Corrosion behavior and surface properties of PVD coatings for mold technology applications,” *Coatings*, vol. 9, no. 1, pp. 1–12, 2019, doi: 10.3390/coatings9010007.

- [49] B. Fotovvati, N. Namdari, and A. Dehghanghadikolaei, “On coating techniques for surface protection: A review,” *J. Manuf. Mater. Process.*, vol. 3, no. 1, 2019, doi: 10.3390/jmmp3010028.
- [50] J. M. Kim, T. H. Ha, I. H. Kim, and H. G. Kim, “Microstructure and oxidation behavior of CrAl laser-coated Zircaloy-4 alloy,” *Metals (Basel)*, vol. 7, no. 2, pp. 1–7, 2017, doi: 10.3390/met7020059.
- [51] W. Zhong, P. A. Mouche, and B. J. Heuser, “Response of Cr and Cr-Al coatings on Zircaloy-2 to high temperature steam,” *J. Nucl. Mater.*, vol. 498, pp. 137–148, Jan. 2018, doi: 10.1016/j.jnucmat.2017.10.021.
- [52] J. C. Brachet *et al.*, “Early studies on Cr-Coated Zircaloy-4 as enhanced accident tolerant nuclear fuel claddings for light water reactors,” *J. Nucl. Mater.*, vol. 517, pp. 268–285, Apr. 2019, doi: 10.1016/j.jnucmat.2019.02.018.
- [53] H. Assadi, F. Gärtner, T. Stoltenhoff, and H. Kreye, “Bonding mechanism in cold gas spraying,” *Acta Mater.*, vol. 51, no. 15, pp. 4379–4394, Sep. 2003, doi: 10.1016/S1359-6454(03)00274-X.
- [54] Y. Yamamoto, B. A. Pint, K. A. Terrani, K. G. Field, Y. Yang, and L. L. Snead, “Development and property evaluation of nuclear grade wrought FeCrAl fuel cladding for light water reactors,” *Journal of Nuclear Materials*, vol. 467, pp. 703–716, 2015, doi: 10.1016/j.jnucmat.2015.10.019.
- [55] Y. Yamamoto, K. Kane, B. A. Pint, A. Trofimov, and H. Wang, “Report on Exploration of New FeCrAl Heat Variants with Improved Properties,” no. August, p. Medium: ED, 2019, [Online]. Available: <https://www.osti.gov/servlets/purl/1558505>.

- [56] J. G. Gigax, J. S. Weaver, and N. Li, "Microstructural Characterization of FeCrAl C26M Tubes," 2018, [Online]. Available:
<https://permalink.lanl.gov/object/tr?what=info%3Aalanl-repo%2Flareport%2FLA-UR-18-27489>.
- [57] E. B. Kashkarov, D. V. Sidelev, M. S. Syrtanov, C. Tang, and M. Steinbrück, "Oxidation kinetics of Cr-coated zirconium alloy: Effect of coating thickness and microstructure," *Corros. Sci.*, vol. 175, Oct. 2020, doi: 10.1016/j.corsci.2020.108883.
- [58] T. Graening, C. P. Massey, K. Linton, and A. Nelson, "Microstructure Investigation and Mechanical Properties of Coated Zircaloy Cladding," p. 31, 2021.
- [59] C. Duriez *et al.*, "Zircaloy-4 high temperature oxidation in atmospheres representative of SFP-LOCA: Investigation of the influence of a low temperature pre-oxidation scale," *J. Nucl. Mater.*, vol. 513, pp. 152–174, 2019, doi: 10.1016/j.jnucmat.2018.10.019.
- [60] J. H. Seong, C. Wang, B. Phillips, and M. Bucci, "Investigation of subcooled flow boiling and CHF on unoxidized and oxidized zircaloy-4 surfaces," 2019.
- [61] S. Wettability, "Standard Test Method for Surface Wettability and Absorbency of Sheeted Materials Using an Automated contact angle tester," vol. 99, no. Reapproved, pp. 1–7, 2003.
- [62] H. H. S. E.S. Gadelmawla, M.M. Koura, T.M.A. Maksoud, I.M. Elewa, "Roughness parameters," *J. Mater. Process. Technol.*, 2002.
- [63] N. Yousif *et al.*, "Filtering and general measruement conditions," *J. Phys. Ther. Sci.*, vol. 9, no. 1, pp. 1–11, 2018, [Online]. Available:

<http://dx.doi.org/10.1016/j.neuropsychologia.2015.07.010><http://dx.doi.org/10.1016/j.visres.2014.07.001><https://doi.org/10.1016/j.humov.2018.08.006><http://www.ncbi.nlm.nih.gov/pubmed/24582474><https://doi.org/10.1016/j.gaitpost.2018.12.007>
tps:

- [64] G. P. Specifications, “ISO 4288,” 1996.
- [65] J. Gabriel, “ISO 4287,” *61010-1* © *Iec2001*, vol. 6, no. 5, p. 13, 2003.
- [66] I. Precision Devices, “Surface Roughness Terminology and Parameters,” *3975-Op Param. Defin.*, 2013, [Online]. Available:
www.predev.com/pdffiles/surface_roughness_terminology_and_parameters.pdf.
- [67] R. V. Umretiya, D. Lee, B. Elward, M. Anderson, R. B. Rebak, and J. V. Rojas, “Evolution of Microstructure and Surface Characteristics of FeCrAl alloys when Subjected to Flow Boiling Testing,” *J. Nucl. Mater.*, vol. 557, p. 153269, 2021, doi: 10.1016/j.jnucmat.2021.153269.
- [68] Y. He, J. Liu, S. Qiu, Z. Deng, Y. Yang, and A. McLean, “Microstructure and high temperature mechanical properties of as-cast FeCrAl alloys,” *Mater. Sci. Eng. A*, vol. 726, no. March, pp. 56–63, 2018, doi: 10.1016/j.msea.2018.04.039.
- [69] R. Umretiya, R. Uhorchuk, S. Vargas, C. E. Castano, and J. Rojas, “Surface characterization of chromium coated zircaloy-4 accident tolerant fuel cladding material,” *Trans. Am. Nucl. Soc.*, vol. 121, no. November, pp. 1811–1812, 2019, doi: 10.13182/T30862.

Vita

Connor F. Donlan

EDUCATION

- **Virginia Commonwealth University (December 2021)**

Masters of Science Candidate in Mechanical Engineering

- **Virginia Military Institute (May 2020)**

Bachelor of Science in Mechanical Engineering